



**HAL**  
open science

## **OSIP1 is a self-assembling DUF3129 protein required to protect fungal cells from toxins and stressors**

Nicolas Valette, Julien Renou, Alexis Boutilliat, Antonio José Fernández-gonzález, Valérie Gautier, Philippe Silar, Christophe Guyeux, Jean-claude Charr, Stéphane Cuenot, Christophe Rose, et al.

### ► To cite this version:

Nicolas Valette, Julien Renou, Alexis Boutilliat, Antonio José Fernández-gonzález, Valérie Gautier, et al.. OSIP1 is a self-assembling DUF3129 protein required to protect fungal cells from toxins and stressors. *Environmental Microbiology*, 2021, 10.1111/1462-2920.15381 . hal-03123656

**HAL Id: hal-03123656**

**<https://hal.science/hal-03123656>**

Submitted on 25 Mar 2021

**HAL** is a multi-disciplinary open access archive for the deposit and dissemination of scientific research documents, whether they are published or not. The documents may come from teaching and research institutions in France or abroad, or from public or private research centers.

L'archive ouverte pluridisciplinaire **HAL**, est destinée au dépôt et à la diffusion de documents scientifiques de niveau recherche, publiés ou non, émanant des établissements d'enseignement et de recherche français ou étrangers, des laboratoires publics ou privés.

1 **OSIP1 is a self-assembling DUF3129 protein required to protect fungal cells from toxins**  
2 **and stressors**

3

4 **Running title: OSIP1 prevent cell wall stress**

5

6 Nicolas Valette<sup>a</sup>, Julien Renou<sup>a</sup>, Alexis Boutilliat<sup>a</sup>, Antonio José Fernández-González<sup>a</sup>,  
7 Valérie Gautier<sup>b</sup>, Philippe Silar<sup>b</sup>, Christophe Guyeux<sup>c</sup>, Jean-Claude Charr<sup>c</sup>, Stéphane Cuenot<sup>d</sup>,  
8 Christophe Rose, Eric Gelhaye<sup>a</sup>, Mélanie Morel-Rouhier<sup>a#</sup>.

9

10 <sup>a</sup>Université de Lorraine, INRAe, Interactions Arbres/Micro-organismes (IAM), UMR 1136,  
11 F-54000 Nancy, France

12 <sup>b</sup>Université Paris Diderot, Sorbonne Paris Cité, Laboratoire Interdisciplinaire des Energies de  
13 Demain (LIED), 75205 Paris, France

14 <sup>c</sup>Computer Science Department, FEMTO-ST Institute, UMR 6174 CNRS, Université de  
15 Bourgogne Franche-Comté, 16 route de Gray, 25030 Besançon, France

16 <sup>d</sup>Institut des Matériaux Jean Rouxel, Université de Nantes, 2 rue de la Houssinière, 44322  
17 Nantes Cedex 3, France

18 <sup>e</sup> Université de Lorraine, AgroParisTech, INRAE, UMR Silva, Nancy, 54000, France.

19

20 <sup>#</sup>**Corresponding author:** Mélanie Morel-Rouhier, Université de Lorraine, UMR1136 INRA-  
21 Université de Lorraine "Interactions Arbres/Micro-organismes", Faculté des Sciences et  
22 Technologies BP 70239, F-54506 Vandoeuvre-lès-Nancy Cedex, France.  
23 Melanie.Morel@univ-lorraine.fr, phone: +33 3 72 74 51 62.

24

25 **Keywords:** OSIP1, fungi, cell wall, stress, oak extractives, secretome

26 **Summary (200 mots)**

27 Secreted proteins are key players in fungal physiology and cell protection against external  
28 stressing agents and antifungals. OSIP1 is a fungal-specific protein with unknown function.  
29 By using *Podospora anserina* and *Phanerochaete chrysosporium* as models, we combined  
30 both *in vivo* functional approaches and biophysical characterization of OSIP1 recombinant  
31 protein. Our data showed an increased sensitivity of the *P. anserina* OSIP1<sup>A</sup> mutant to both  
32 caspofungin and oak-extractives. This correlated with the weakened extracellular matrix  
33 produced by the mutant compared to the wild type, as highlighted by SEM imaging. This  
34 alteration quantitatively modified the global secretome of *P. anserina* grown in presence of  
35 wood, such as proteins associated to the cell-wall integrity signaling pathway. Since the  
36 recombinant OSIP1 from *P. chrysosporium* self-assembled as fibers and was capable of  
37 gelation, these results argue for a structural role of OSIP1 proteins in fungi at the cell wall or  
38 within the matrix conferring cell protection against external toxic compounds. These data  
39 could be of great interest for increasing protein secretion in a context of lignocellulosic  
40 biomass degradation, such as improving the efficiency of antifungals that could be trapped  
41 within the extracellular matrix.

42

43

44

## 45 **Introduction**

46 During evolution, fungi had to adapt to environmental constraints. The secretome, *i.e.* the  
47 proteins secreted in the extracellular medium, is a good marker of fungal physiology and  
48 trophic modes. Indeed, the secretome is involved in the first steps of the symbiosis or  
49 infection establishment and plays essential roles in plant biomass degradation (Kämper *et al.*,  
50 2006; Bouws *et al.*, 2008; Vincent *et al.*, 2012). Fungal secretomes are composed of  
51 degradative enzymes such as proteases, lipases, Carbohydrate-Active enZymes (CAZymes),  
52 and ligninolytic enzymes for some wood-decaying species (Zhu *et al.*, 2016; Pellegrin *et al.*,  
53 2015). This degradative system has been intensively studied due to its important application  
54 in lignocellulose biomass valorization. In plant-associated fungi, other proteins can be  
55 secreted to modulate plant immunity and establish symbiosis or allow pathogenic infection  
56 (Plett *et al.*, 2011; Pazzagli *et al.*, 1999; Frias *et al.*, 2011; Baccelli *et al.*, 2014). Some of  
57 them, the hydrophobins, are involved in the attachment of fungal structures to different kinds  
58 of surfaces and the development of hyphae at the water/air interface (Wessels *et al.*, 1991;  
59 Wessels, 1996). In fungal pathogens, hydrophobins might act as virulence factors to enhance  
60 fungal infection (Ruocco *et al.*, 2015; Kubicek *et al.*, 2008), while in symbiotic associations,  
61 these proteins could be involved in mycorrhizae formation (Plett *et al.*, 2012). Most of the  
62 studied hydrophobins are directed to the extracellular medium through the secretory pathway.  
63 However, they often remain associated with the fungal cell wall and can be found inside  
64 fruiting bodies and on the surfaces of hyphae, spores and conidia (Dynesen *et al.*, 2003;  
65 Linder, 2009). Many other secreted proteins have been identified but remain of unknown  
66 function. This is the case for SSP (for Small Secreted Proteins with sequence less than 300  
67 amino acids) (Alfaro *et al.*, 2014). The percentage of SSP-coding genes in the genomes of  
68 saprophytic fungi such as *Phanerochaete chrysosporium*, *Trametes versicolor* or *Aspergillus*  
69 *fumigatus* is similar to the one of the ectomycorrhizal fungus *Laccaria bicolor* (between 2 and

70 3 % of the predicted gene models) (Pellegrin *et al.*, 2015; Valette *et al.*, 2016). At the protein  
71 level, SSPs represent between 4 and 12% of the proteins identified in the secretomes of  
72 various *Aspergillus* species grown on sugar beet pulp or wheat bran (Valette *et al.*, 2016).  
73 However, only few have been functionally characterized. One SSP of the lignolytic fungus  
74 *Pleurotus ostreatus* is involved in the regulation of the lignolytic system by modulating  
75 expression and activity of aryl-alcohol oxidases, aryl-alcohol dehydrogenases and versatile  
76 peroxidases (Feldman *et al.*, 2017) and in the transition from primary to secondary  
77 metabolism, development, aging, and fruiting body initiation (Feldman *et al.*, 2019).  
78 In a previous analysis, we have highlighted the up-regulation of various SSP-coding genes of  
79 the lignolytic fungus *Phanerochaete chrysosporium* in presence of oak extractives (Thuillier  
80 *et al.*, 2014, Fernández-González *et al.*, 2018). Oak extractives are mainly composed of  
81 phenolic compounds and flavonoids (Zhang *et al.*, 2015; Fernández-González *et al.*, 2018).  
82 These molecules are released from wood during the degradative process and can be toxic for  
83 cells by various mechanisms such as metal and free radical scavenging activity, direct  
84 interaction with enzymes, perturbation of ionic homeostasis and disruption of membrane and  
85 cell wall integrity (Valette *et al.*, 2017). One of these up-regulated genes retained our attention  
86 because the corresponding protein was also detected at high amount in the secretome of  
87 another white rot fungus *Trametes versicolor* grown on oak wood chips (Deroy *et al.*,  
88 unpublished). This protein was thus named OSIP1 for Oak Stress Induced Protein. It shows  
89 no sequence homology with characterized proteins in the databases. In this study we used two  
90 fungal models to decipher the role of OSIP1: *Podospora anserina* for functional analysis  
91 because genetic engineering is easy, contrary to *P. chrysosporium* or *T. versicolor*; and *P.*  
92 *chrysosporium* for the biochemical analysis because only PcOSIP1 was successfully produced  
93 as a recombinant protein.

94

95 **Results**

96 **Comparative genomic analysis reveals that OSIP1 is widespread in fungi**

97 OSIP1 sequences from the ascomycete *P. anserina* (*PaOSIP1*: ProtID JGI 208230, a.k.a.  
98 Pa\_5\_3780 according to the *P. anserina* genome project) and the basidiomycete *P.*  
99 *chryso sporium* (*PcOSIP1*: ProtID JGI 2981896) were used as templates to search for fungal  
100 sequences using the BlastP search tool onto the whole fungal JGI database (Mycocosm from  
101 Joint Genome Institute). The sequence of *P. anserina* P209725 (ProtID JGI 209725) was also  
102 used as template since it displays 38% similarity with *PaOSIP1*). A total of 1057 protein  
103 sequences were retrieved and analyzed by clustering. These sequences grouped into nine  
104 clusters (Fig. 1A). *PaOSIP1* and *PcOSIP1* belonging to cluster 1, this latter was thus named  
105 OSIP1 cluster (species and accession numbers are available in Table S1). It gathers sequences  
106 from both ascomycetes (*Pezizomycotina*) and basidiomycetes (*Agaricomycotina* and  
107 *Pucciniomycotina*). Moreover, this analysis revealed that *OSIP1* is present in genomes of  
108 wood decay fungi, and also in mycorrhizal, pathogenic fungi and other saprotrophs (Fig. 1A).  
109 Although OSIP1 was found induced by oak extractives in lignolytic fungi (Thuillier *et al.*,  
110 2014; Deroy, unpublished), this genomic analysis showing that OSIP1 is present in fungi with  
111 various trophic modes, argues against its direct involvement in the lignolytic process and  
112 suggests a more general role in fungal physiology.

113

114 **OSIP1 sequences contain a DUF3129 domain, like some appressoria-specific proteins**

115 OSIP1 sequences exhibit a signal peptide of secretion, a conserved DUF3129 domain and a  
116 variable C-terminal tail (Fig. 1B). In ascomycetes, 8 cysteinyl residues are conserved, while  
117 only four have been detected in the analyzed basidiomycete sequences (Fig. 1B and Fig S1).  
118 The DUF3129 domain is not restricted to OSIP1 sequences. It can be identified in both  
119 ascomycetes and basidiomycetes and was retrieved in 442 sequences from the Pfam 31.0

120 database. Although most of the proteins having the DUF3129 are annotated as  
121 uncharacterized proteins, some of them are described as being related to CAS1  
122 (*Colletotrichum gloeosporioides* appressoria-specific protein), MAS (*Magnaporthe*  
123 appressoria-specific protein), gEgh16 from *Blumeria graminis* proteins, all being putatively  
124 involved in fungal cell wall remodeling. A phylogenetic analysis was performed with the  
125 sequences from the OSIP1 cluster and the 442 sequences containing the DUF3129 domain  
126 (Fig. 1C). PaOSIP1 clusters with ascomycete sequences but independently of CAS1 from *C.*  
127 *gloeosporioides*, MAS3 from *M. grisea* and gEgh16 from *B. graminis*. Among  
128 basidiomycetes, sequences from *Agaricomycotina* with lignolytic, saprotrophic or  
129 mycorrhizal lifestyles (Group A) cluster independently from sequences of pathogenic  
130 basidiomycetes from *Pucciniomycotina* and *Agaricomycotina* (Group B) (details are given in  
131 Table S1).

132

### 133 **PaOSIP1 maintains cell wall integrity under caspofungin stress**

134 To functionally characterize OSIP1, the OSIP1 knock-out mutant was generated in *P.*  
135 *anserina* (*PaOSIP1<sup>Δ</sup>*) (Fig S2). *PaOSIP1<sup>Δ</sup>* was tested for its ability to grow on various carbon  
136 sources (cellobiose, fructose, cellulose, pectin, glucose) and various biomasses (whatman  
137 paper, hay, miscanthus, wood chips). No differences in growth, sporulation, nor appressoria-  
138 like structure formation (as described in Brun *et al.*, 2009) was highlighted between the wild  
139 type and the *PaOSIP1<sup>Δ</sup>* mutant strains in the tested conditions (data not shown). Because the  
140 DUF3129 domain is present in cell wall remodeling proteins, cell wall destabilizing agents  
141 were thus tested. No phenotype was observed for Congo red that prevents glucan microfibril  
142 assembly mainly by binding  $\beta$ -1,3 glucans (Nodet *et al.*, 1990) nor Calcofluor white, which  
143 binds chitin. By contrast, a significant deleterious growth phenotype was observed for the  
144 mutant compared to the wild type in presence of caspofungin (Fig. 2). Caspofungin is a cell

145 wall-targeting antifungal compound extensively used in clinical settings for the treatment of  
146 infections caused by diverse fungi. Caspofungin inhibits the synthesis of  $\beta$ -1,3-glucan, a  
147 crucial cell wall component for many fungi, by targeting the  $\beta$ -1,3-glucan synthase (encoded  
148 by *fks1*) in a non-competitive way (Van Den Bossche, 2002; Aguilar-Zapata *et al.*, 2015).  
149 Functional complementation of *PaOSIP1<sup>Δ</sup>* by PaOSIP1 restored the growth defect confirming  
150 the role of PaOSIP1 in protecting cell wall under caspofungin treatment.

151

### 152 ***PaOSIP1<sup>Δ</sup>* mutant is affected in extracellular matrix production**

153 To check whether caspofungin sensitivity was due to a thinner cell wall in the mutant  
154 compared to the wild type, SEM imaging was performed after cryosection of the hyphae (Fig.  
155 3). The whole reconstituted images are shown as supplementary data. The thickness of the  
156 cell wall was measured (n>50) based on the microscopic images. No difference was detected  
157 between the WT and the mutant, nor between the caspofungin and the control condition. The  
158 measured cell wall thickness of hyphae cross-sections was around 150 nm for all conditions  
159 analysed. Interestingly, the main difference highlighted by comparing SEM images of both  
160 mutant and WT strains was the extracellular matrix (ECM) density. Fungal extracellular  
161 matrix is mainly composed of carbohydrates and proteins in complex interactions. This matrix  
162 is strongly reduced in *PaOSIP1<sup>Δ</sup>* even in the absence of caspofungin (Fig. 3). Since this  
163 matrix was shown to prevent drugs from reaching their cellular targets (Mitchell *et al.*, 2016),  
164 this could explain why *PaOSIP1<sup>Δ</sup>* showed an increased sensitivity to the antifungal  
165 caspofungin.

166

### 167 **Recombinant OSIP1 self-assembles as fibers and forms a gel**

168 The heterologous *Escherichia coli* system was tested for recombinant PaOSIP1 and PcOSIP1  
169 productions. Only PcOSIP1 expressed in *E. coli* was successfully produced. After

170 purification, 3 mg of pure protein per liter of bacterial culture were obtained. To check  
171 whether the protein was correctly folded, far-UV circular dichroism analysis was performed.  
172 Spectrum of PcOSIP1 revealed secondary structures, mainly alpha helices as highlighted by a  
173 positive band at 190 nm and two negative bands at 208 and 222 nm (Fig. 4A).

174 After purification, PcOSIP1 rapidly self-assembled as big oligomers in Tris-NaCl buffer (30  
175 mM Tris-HCl pH 8.0, 200 mM NaCl), as shown by dynamic light scattering (DLS) analysis  
176 (Fig. 4B). Huge hydrodynamic radii ( $R_h$ ) of  $789.3 \pm 388$  nm and  $2\ 281 \pm 880$  nm were  
177 respectively measured for 56.7% and 28.7% of the PcOSIP1. This aggregation was not  
178 observed when the protein was dialyzed in 50 mM phosphate buffer pH 8.0 directly after  
179 purification, suggesting that this process was driven by the physicochemical properties of the  
180 buffer. To check whether this aggregation was due to protein instability and thus precipitation  
181 or rather a specific organization, the macromolecular structures of PcOSIP1 was analyzed by  
182 Atomic Force Microscopy (AFM). In Tris-NaCl buffer, PcOSIP1 was able to self-assemble  
183 into fibers with a mean diameter of  $1.5 \pm 0.2$  nm (Fig. 4C). In phosphate buffer, a crown  
184 structure was evidenced. This crown organization could be the transient states of PcOSIP1  
185 fibril formation, since such structure was already described in transient states of the human  $\alpha$ -  
186 synuclein fibril formation that contributes to Parkinson's disease (Lashuel *et al.*, 2002 ; Apetri  
187 *et al.*, 2006).

188 All the experiments described above were performed directly or few days after protein  
189 purification. Interestingly, storing PcOSIP1 in Tris-NaCl buffer in the freezer led to the  
190 formation of a gel, that was quite compact and elastic (Fig. 4D). This specific feature was  
191 already described for other proteins as  $\alpha$ -synuclein that can form gels in buffer at pH 7.4 in  
192 the presence of NaCl (Semerdzhiev *et al.*, 2018). These atypical properties of self-assembly  
193 and jelly structure formation support a putative structural role of OSIP1 protein within the  
194 fungal cell wall or the extracellular matrix.

195

### 196 **Oak-extractives affect *PaOSIP1<sup>Δ</sup>* growth**

197 During wood degradation, extractives act as important stressors for fungal cells (Thuillier *et*  
198 *al.*, 2014 ; Valette *et al.*, 2017 ; Fernández-González *et al.*, 2018). Some of them can act  
199 directly on cell wall integrity. For example, similarly to caspofungin, cinnamaldehyde and  
200 poacic acid inhibit  $\beta$ -1,3-glucan synthesis within the fungal cell wall (Bang *et al.*, 2000;  
201 Piotrowski *et al.*, 2015). Because OSIP1 gene expression was induced by oak extractive-  
202 induced stress both in *P. chrysosporium* (Thuillier *et al.*, 2014) and *P. anserina* (data not  
203 shown), this condition was used to test *PaOSIP1<sup>Δ</sup>* growth phenotype. The results showed a  
204 growth delay of *PaOSIP1<sup>Δ</sup>* compared to the wild type in presence of wood extractives, which  
205 was observable from 5 days (Fig. 5). This phenotype was partially restored by functional  
206 complementation with PaOSIP1. These results support the hypothesis that PaOSIP1 could  
207 participate in cell wall protection against extractives toxicity.

208

### 209 **The deletion of OSIP1 strongly modifies the composition of the secretome and the cell-** 210 **wall related proteins of *P. anserina* in presence of oak sawdust**

211 To analyze how the deletion of PaOSIP1 affects the fungal physiology in a context of biomass  
212 degradation, a proteomic analysis was performed for the *PaOSIP1<sup>Δ</sup>* mutant grown in presence  
213 of oak sawdust, in comparison with the wild type strain. The comparative analysis of the  
214 secreted proteins reveals strong modification of the global secretome of *PaOSIP1<sup>Δ</sup>* mutant  
215 compared to the wild type strain (Fig. 6A). Indeed, over the 250 proteins detected, 150 were  
216 more abundant (Protein abundance index (PAI) fold>2) or specifically identified in the mutant  
217 compared to the wild type, while this number was only 41 in the case of the wild type.

218 By looking at the various classes of enzymes that were more abundant in the mutant  
219 secretome compared to the WT, no clear specificity was observed except for proteases that

220 were less represented (Fig. 6B). Globally, more than half (around 60%) of the detected  
221 proteins of a specific class were more abundant in the secretome of the mutant compared to  
222 the wild type. It is likely that the deletion of OSIP1 globally affected the secretion process of  
223 the enzymes.

224 Glycoside hydrolases (GH) were the most abundant proteins with a total of 66 GH detected in  
225 both secretomes. By looking at the individual GH families, we showed again that the increase  
226 in protein abundance is not restricted to specific families, but was observed for many of them  
227 (Fig. 6C). However, it is interesting to note that 16 GH families (over the total of 29) were  
228 specifically detected in the mutant strain, especially GH5, GH11 and GH43 with at least 3  
229 isoforms.

230 A high number of cell wall-related proteins, in particular glucan-acting enzymes have also  
231 been found more abundant in the secretome of the mutant strain (Fig. 6D). Moreover, many  
232 Wall Stress responsive Component (WSC) proteins have been detected. These proteins serve  
233 as sensors of external stress cues upstream of cell wall integrity (CWI) pathway in  
234 *Saccharomyces cerevisiae* (Verna *et al.*, 1997) and *Aspergilli* (Futagami *et al.*, 2011; Dichtl *et*  
235 *al.*, 2012). In line with this observation, respectively 3 and 6 DUF1996-containing proteins  
236 were found more abundant and specifically detected in the mutant among the 10 detected in  
237 total (Supplementary data). These proteins are of unknown function, however the DUF1996  
238 domain has been associated to fungal stress sensing and response (Tong *et al.*, 2016a and  
239 2019).

240

## 241 **Discussion**

242 In this study, we characterized a new fungal protein, which participates in cell wall fitness  
243 under stress. The comparative genomic analysis revealed that such proteins are widely present  
244 in fungi, suggesting their involvement in a general process of stress rescue. All analyzed

245 OSIP1 possess a domain of unknown function DUF3129 that was previously identified by  
246 few studies in proteins of both plant and insect pathogens (Shang *et al.*, 2016). DUF3129 is an  
247 expanded gene family highly expressed during infection in nematode-trapping fungi that form  
248 adhesive branches and adhesive knobs (Andersson *et al.*, 2014). The role of this domain was  
249 attributed to the cell wall remodeling for fungal penetration to host cuticles with an unclear  
250 mechanism (Justesen *et al.*, 1996 ; Xue *et al.*, 2002 ; Grell *et al.*, 2003 ; Cao *et al.*, 2012).  
251 More recently, seven DUF3129 proteins of the insect pathogenic fungus *Metarhizium*  
252 *robertsii* were found localized to cellular lipid droplets mediating their degradation and  
253 subsequently controlling appressorial turgor required for infection (Huang *et al.*, 2019).  
254 However, nothing has been described concerning the role of these DUF3129-containing  
255 proteins in saprophytic fungi. The jelly structure of the recombinant PcOSIP1 and the  
256 reduction of the extracellular polysaccharide network observed for the PaOSIP1 mutant  
257 strongly suggest the involvement of OSIP1 in the formation of such adhesive structures in  
258 fungi. The weakened extracellular matrix of the mutant could thus be responsible for the  
259 higher susceptibility of the fungus to both caspofungin and oak extractives.

260 This phenomenon has been already described in *A. fumigatus*, where the downregulation of a  
261 hydrophobin gene by a polyphenolic compound resulted in a weakened extracellular matrix  
262 and therefore increased the susceptibility of the fungi to antifungal drugs (Luo *et al.*, 2018).  
263 Hydrophobins are small (100–120 aa) secreted proteins characterized by the presence of eight  
264 highly conserved cysteine residues and the ability to self-assemble as amyloid-like structure  
265 and forms rodlets (Ball *et al.*, 2020). Amyloids serve diverse purposes for structure, adhesion  
266 and defence in microorganisms (Shanmugam *et al.*, 2019) and can be evidenced *in vitro* using  
267 fluorescent tool as thioflavin T, which binds to the beta sheet-rich structure characteristic of  
268 amyloid-like structure (Groenning, 2010). PcOSIP1 does not assemble under amyloid  
269 structure since no thioflavin T fluorescence signal was detected in any of the conditions of

270 temperatures and buffers tested (data not shown). We have shown that PcOSIP1 was rich in  $\alpha$ -  
271 helices, while amyloid is structurally dominated by  $\beta$ -sheets. Moreover, AFM revealed that it  
272 did not form rodlets. These experimental data, coupled to sequence analysis, allowed us to  
273 confirm that OSIP1 is a new self-assembling protein, that does not belong to the well-known  
274 class of hydrophobins.

275 In the context of lignocellulosic biomass degradation, the structural property of OSIP1 may be  
276 the key point explaining the way by which it participates in fungal stress resistance by  
277 protecting the cell wall. In accordance, the comparative secretome analysis of *P. anserina*  
278 grown on oak sawdust revealed that the *PaOSIP1*<sup>Δ</sup> mutant highly expresses WSC proteins  
279 compared to the wild type in this condition. WSC proteins are localized to the cell wall and  
280 the plasma membrane and act as sensors upstream of the cell-wall integrity pathway. In  
281 particular, WSC-1 may function in regulating cell wall biogenesis through the MAK-1  
282 pathway in *Neurospora crassa* (Maddi *et al.*, 2012). Single deletions of the five *wsc* genes of  
283 *Beauveria bassiana* resulted in significant, but differential, increases in cellular sensitivity to  
284 cell wall perturbation, oxidation, high osmolarity, and metal ions (Tong *et al.*, 2016b). In  
285 *Aspergillus fumigatus*, deletions of *wsc1* caused an increased in sensitivity to caspofungin but  
286 no change in cellular sensitivity to other cell wall perturbation, alkaline pH and high  
287 temperature (Dichtl *et al.*, 2012). In the nematode-trapping fungus *Monacrosporium*  
288 *haptotylum*, a gene cluster of 5 secreted proteins that are adjacent in the *M. haptotylum*  
289 genome (cluster 74) is highly (>10-fold) upregulated during infection (Andersson *et al.*,  
290 2013). This cluster gathers two genes coding for WSC proteins, one gene containing the  
291 DUF3129 domain and two SSP-coding genes (Meerupati *et al.*, 2013). This suggests a  
292 functional link between these proteins. Additionally to WSC proteins, the *PaOSIP1*<sup>Δ</sup> mutant  
293 highly expresses DUF1996-containing proteins. In *B. bassiana*, DUF1996-containing proteins  
294 localize in vacuoles and play significant roles in the response to cell-wall perturbation, high

295 osmolarity, oxidation, fungicidal and multiple metal stress (Tong *et al.*, 2016a). The absence  
296 of OSIP1 in *P. anserina* grown in presence of oak sawdust strongly affected the whole  
297 secretome of the fungus, likely because of the cell wall weakness. Indeed, the functionality of  
298 the cell wall integrity (CWI) and secretory systems are connected and coordinately respond to  
299 exogenous stresses through the modulation of the cell periphery and secretion (Malavazi *et*  
300 *al.*, 2014).

301 Taking together, these data strongly suggest that OSIP1 proteins prevent cell wall stress.  
302 Consequently, its absence affects the cell wall associated signaling pathway, leading to a  
303 deregulation of the secretion process. These data could be of great interest for both the  
304 improvement of protein secretion particularly in a context of lignocellulosic biomass  
305 degradation, and the limitation of fungal pathogenicity, for which the fungal cell wall has a  
306 crucial role (Gow *et al.*, 2017).

307

## 308 **Experimental procedures**

### 309 **Growth conditions**

310 The *P. anserina* strain used in this study was derived from the S strain (Rizet, 1952; Boucher  
311 *et al.*, 2017). Standard culture conditions, media compositions and genetic methods for this  
312 fungus have already been described (Rizet, 1941; Silar, 2013) and are available at  
313 <https://podospora.i2bc.paris-saclay.fr>. Growth kinetics of the wild type and *PaOSIP1*<sup>Δ</sup> strains  
314 were done in M2-Agar medium and M2-Agar medium supplemented with caspofungin (500  
315 ng/ml) and oak extractives (2 mg/ml) for 10 days at 27 °C. Oak (*Quercus petraea*) acetic  
316 extract preparation has been performed as described previously (Fernández-González *et al.*,  
317 2018).

318

### 319 **Analysis of OSIP1 sequences**

320 OSIP1 sequences were searched within all fungal genomes available in the Joint Genome  
321 Institute database (Mycocosm <https://genome.jgi.doe.gov/programs/fungi/index.jsf>) using  
322 BlastP with a cut off of  $Evalue=10^{-5}$ . Sequences of OSIP1 of *Podospora anserina* ((PaOSIP1  
323 (208230 JGI) and *Phanerochaete chrysosporium* (ProtID 2981896 JGI) have been used as  
324 templates. Another sequence close to PaOSIP1 was added as a template (P209725 (ProtID  
325 209725 JGI)). Evolutionary analyses were conducted in MEGA7 using the Neighbor-Joining  
326 method (Kumar *et al.*, 2016). The tree is drawn to scale, with branch lengths in the same units  
327 as those of the evolutionary distances used to infer the phylogenetic tree. The evolutionary  
328 distances were computed using the Poisson correction method and are in the units of the  
329 number of amino acid substitutions per site. The analysis involved 628 amino acid sequences.  
330 All ambiguous positions were removed for each sequence pair. There were a total of 467  
331 positions in the final dataset. To carry out the clustering, the Laplacian eigenmap technique  
332 (Belkin and Niyogi, 2003) was applied with Gaussian mixture model (Reynolds, 2015) as  
333 follows. After sorting the sequences in alphabetical order, the similarity of each sequence pair  
334 were obtained from the score provided during a pairwise sequence alignment using the  
335 Needleman-Wunsch (Needleman and Wunsch, 1970) dynamic programming algorithm from  
336 Biopython (Cock *et al.*, 2009) module (pairwise2 function). Default values for gap open and  
337 extend penalties were chosen with blosum62 matrix for amino acid substitution, leading to a  
338 matrix  $M$  of integers. A similarity matrix  $S$  has been deduced by dividing each row by its  
339 maximum, and by computing the identity matrix minus this one. The normalized Laplacian  
340 associated with the similarity matrix has been computed as follows:  $L = D^{-1}(D-S)$ , where  $D$  is  
341 the diagonal matrix whose element in position  $(i,i)$  is the sum of the  $i$ -th row in  $S$ . Eigenvalues  
342 of  $L$  have then been computed and sorted in ascending order thanks to the numpy library  
343 (Oliphant, 2006), and the  $N$ -th first eigenvalues have only be considered, where  $N$  is such that  
344 the increase between the  $N$ -th and  $N+1$ -th eigenvalue is lower than 1%. Associated

345 eigenvectors have then been clusterized according to a Gaussian mixture model (Reynolds,  
346 2015), and the model selection (number of Gaussians) has been performed according to the  
347 Bayesian Information Criterion (BIC, (Schwarz, 1978)). To sum up, Laplacian eigenmap  
348 allowed us to map the similarity matrix in a low dimensional space of points, each point being  
349 associated to one amino acid sequence. This cloud points has been considered as the  
350 superposition of a given number of gaussian trends (the clusters), this number being  
351 determined thanks to the BIC criterion of parcimony. For further information about this  
352 sequence clustering technique, see, e.g. Bruneau *et al.* (2018).

353

#### 354 **Deletion of PaOSIP1 in *Podospora anserina***

355 To delete PaOSIP1 (Pa\_5\_3780), the “split marker” method was used (Silar, 2013). This  
356 protocol is based on the generation of two DNA fragments carrying a resistance marker  
357 flanked with either 5’ or 3’ non-coding sequence of the genes by two successive PCR  
358 reactions. In the first step, a 832 pb-long 5’-non-coding region of PaOSIP1 and a 962 pb-long  
359 3’ region were PCR-amplified from the S strain DNA with the PaOSIP1-A/ PaOSIP1-B, and  
360 PaOSIP1-C/ PaOSIP1-D primer pairs respectively. At the same time, the hygromycin  
361 resistance marker was amplified with PaOSIP1-E and PaOSIP1-F from the pBC-hygro vector  
362 (Silar, 1995). Primers sequences are given in Fig. S2. In a second step, the second round of  
363 PCR using primers PaOSIP1-A and PaOSIP1-F, and PaOSIP1-D and PaOSIP1-E enabled to  
364 merge the resistance marker with either the 5’ or the 3’ region. The two PCR products were  
365 used to transform a mus51::phleoRstrain, in which the mus51 gene encoding one of the  
366 subunit of the non-homologous end joining dimer is replaced with a phleomycin resistance  
367 gene. Three crossing-over events between the two cassettes and the *P. anserina* genome  
368 enabled the deletion of PaOSIP1. Three hygromycin resistant transformants were selected.  
369 They were crossed with the wild-type S strain, and one homokaryotic hygromycin resistant

370 and phleomycin-sensitive descendant was selected as the PaOSIP1::hygroRstrain or  
371 *PaOSIP1*<sup>Δ</sup>. Its genotype was confirmed by Southern blot analyses using digoxigenin labeled  
372 probes (Fig. S2). For functional complementation tests, PaOSIP1 coding sequence was cloned  
373 into pAKS-Genet<sup>R</sup> vector and expressed in *PaOSIP1*<sup>Δ</sup>. The presence of the gene was checked  
374 by PCR and three transformants were selected for functional complementation tests. They all  
375 restored the mutant phenotype, thus, only the results for one of them are presented.

376

### 377 **SEM imaging of *PaOSIP1*<sup>Δ</sup> hyphal network**

#### 378 **Cloning of PcOSIP1**

379 *Phanerochaete chrysosporium* mycelium was harvested from liquid cultures in TK medium  
380 supplemented with oak extractives as previously described (Thuillier *et al.*, 2014). Total RNA  
381 was extracted and purified using the RNeasy plant minikit (Qiagen) according to the  
382 manufacturer's instructions. RNA was treated with DNase I during purification as  
383 recommended in the manufacturer's protocol. An additional purification step was performed  
384 by precipitating RNA with 2 M LiCl. RNAs were reverse transcribed using the masterscript  
385 kit (5 prime) following the manufacturer's protocol. The PCR reactions to amplify PcOSIP1  
386 (Prot ID 2981896 in the Joint Genome Institute database v2.2 (previously identified as Prot ID  
387 4474 in v2.0 of *P. chrysosporium* genome annotation)), have been performed with Herculase  
388 Taq (Agilent technologies) for cloning into the pEt26b (Novagen) vector for His-tagged  
389 protein production in *Escherichia coli*. The sequence was amplified without the predicted  
390 signal peptide of secretion using the following primers (for:  
391 CCCCCATATGGCTATTATCACGCCCGCG and rev:  
392 CCCC GCGGCCGCTGCTTGGAGCTCCTCATC).

393

394 **Heterologous expression of PcOSIP1 in *Escherichia coli* and purification of the**  
395 **recombinant protein**

396 Expression of recombinant PcOSIP1 was performed in *E. coli* Rosetta2 (DE3) strain  
397 containing pLysS plasmid ( $F^-$  ompT hsdS<sub>B</sub>(rB- mB-) gal dcm (DE3) pRARE2 (CamR)). The  
398 bacteria were cultivated in LB medium supplemented with 50µg/ml kanamycin and 50µg/ml  
399 chloramphenicol at 37°C. At OD<sub>600</sub> of 0.6, the expression of the recombinant proteins was  
400 induced by adding 0.1 mM isopropyl β-D-1 thiogalactopyranoside (IPTG) during 4h. Cells  
401 were harvested by centrifugation and resuspended in 30 mM Tris-HCl pH 8.0, 500 mM NaCl  
402 buffer and stored at -20°C. The purification of His-tagged PcOSIP1 was performed by affinity  
403 chromatography on IMAC columns (Sigma Aldrich) from the soluble fraction obtained after a  
404 30 min centrifugation (27,000 x g) of cells lysed by sonication. The washing buffer was 30  
405 mM Tris-HCl pH 8.0, 2 M NaCl in a first step and 30 mM Tris-HCl pH 8.0, 500 mM NaCl  
406 and 10 mM imidazole in a second step. The elution buffer was 30 mM Tris-HCl pH 8.0, 500  
407 mM NaCl, 250 mM imidazole. Both proteins were dialyzed against a 30 mM Tris-HCl pH  
408 8.0, 500 mM NaCl buffer by ultrafiltration on YM10 membranes, concentrated and loaded on  
409 Sephadex 75 16/600 column (AKTA purifier) equilibrated with 30 mM Tris-HCl, 200 mM  
410 NaCl. The purified protein was finally concentrated and analyzed on 15% SDS-PAGE gel to  
411 check the purity. The concentration of the protein was determined by BC assay (interchim).

412

413 **Circular dichroism (CD)**

414 Due to the incompatibility of Tris buffer, which absorbs between 180 and 260 nm, the  
415 PcOSIP1 spectrum was recorded exclusively in phosphate buffer. Directly after purification,  
416 PcOSIP1 was dialyzed in 50 mM phosphate buffer pH 8.0 using dialysis membrane  
417 (Spectra/Por, MWCO 6-8 000). Circular Dichroism spectra of PcOSIP1 was obtained in 50  
418 mM phosphate buffer pH 8.0 at 25 °C in a quartz cuvette (1-mm path length) from 180 to 260

419 nm with a bandwidth of 1 nm using a Chirascan Plus spectropolarimeter (Applied  
420 Photophysics, Ltd, UK). The mean residue ellipticity  $[\theta]_{MR}$  was calculated using Pro-Data  
421 Viewer (Applied Photophysics, Ltd, UK) software and expressed in  $\text{deg. cm}^2.\text{dmol}^{-1}$  per  
422 residue.

423

#### 424 **Dynamic Light Scattering (DLS)**

425 The homogeneity of solutions, the aggregation state and particle sizes were analyzed by  
426 granulometry on a Zetasizer Nano-S model (Malvern Instruments, Malvern, UK). The protein  
427 solution was analyzed by DLS at a final concentration of 4mg/ml either in 50 mM phosphate  
428 buffer pH8.0 or 30 mM Tris-HCl, 200 mM NaCl buffer. The supernatant of each sample was  
429 gently transferred into a quartz cuvette of 12  $\mu\text{l}$  and the particle size measurements were  
430 performed in triplicate at 37°C, with alight diffusion at 173°. The data were collected in  
431 automatic mode and analyzed using the associated software DTS version 4.2 (Malvern  
432 Instruments).

433

#### 434 **Atomic Force Microscopy (AFM)**

435 PcOSIP1, either in 50 mM phosphate buffer (pH 8.0) or 30 mM Tris-HCl and NaCl 200 mM  
436 buffer (pH 8.0), was analyzed at a starting protein concentration of 6 mg/ml. The protein  
437 solutions were carefully dialyzed to remove NaCl and diluted 10 times just prior to AFM  
438 observations. A glass coverslip was cleaned with a piranha treatment and washed in ultrapure  
439 water, before being dried in a stream of nitrogen gas. A tiny droplet of each diluted protein  
440 solution was deposited onto the glass coverslip heated at 20°C to promote a rapid drying  
441 (within 2 minutes) while avoiding the formation of concentration gradients on the substrate  
442 (Zykwinska *et al.*, 2014). The sample was then immediately imaged by AFM. A  
443 NanoWizard® Atomic Force Microscope (JPK, Germany) operating in intermittent contact

444 mode under ambient conditions was used to image the protein solutions deposited onto the  
445 glass coverslip. A standard rectangular cantilever (Nanosensors NCL-W) was employed for  
446 imaging (scan rate of 0.5 Hz), with a free resonance frequency of 174 kHz and a curvature  
447 radius of the tip of 10 nm. In order to check the reproducibility of the observed morphology,  
448 all samples were scanned at least on three different zones. Each sample was investigated using  
449 fresh tips previously cleaned by UV-ozone treatment. The height measurements were done  
450 using JPK Data Processing software (JPK, Germany).

451

#### 452 **LC-MS/MS protein identification**

453 *P. anserina* wild type and *PaOSIP1*<sup>Δ</sup> strains were cultivated in flasks containing 1 g of oak  
454 sawdust and 10 ml of M2 medium without any carbon source for 1 month at 25°C. For each  
455 strain, three independent cultures were pooled before protein extraction. Proteins from the  
456 whole sample (sawdust containing mycelium and secretome) were extracted with 10 ml of 50  
457 mM sodium acetate pH4.5 buffer for 1.5 h under shaking at 4°C. The sample was centrifuged,  
458 concentrated with centricon filter membrane (5 kDa) until around 3 ml and precipitated with  
459 cold acetone (80%). 10 µg of proteins was loaded on 12% SDS-PAGE gel. After a short  
460 migration (0.5 cm) in the stacking gel, the gels were stained with Coomassie blue and each  
461 electrophoresis track was cut into two 2-mm-wide strips. Proteomic identification was  
462 performed at the Plate-forme d'Analyse Protéomique de Paris Sud-Ouest (PAPPSO, INRA,  
463 Jouy-en-Josas, France; <http://pappso.inra.fr/>), according to a protocol described in Navarro et  
464 al. (2010). Briefly, the digestion of the proteins contained in the gel strips was carried out  
465 according to a standard trypsinolysis process, using modified trypsin (Promega,  
466 Charbonnières-les-Bains, France). Peptide analysis was performed by Ultimate 3000  
467 RSLCnano liquid chromatography (Thermo Fisher Scientific, Waltham, Massachusetts, USA)  
468 coupled to a Q-exactive mass spectrometer (Thermo Fisher Scientific) using electrospray

469 ionization. Peptide attribution and protein annotation were performed by comparing mass  
470 spectrometry data to predicted proteins in the genomes of *P. anserina* as well as an internal  
471 contaminant database, using X!Tandem Cyclone software (X!Tandem, Jouy-en-Josas,  
472 France). The protein annotation was completed manually by BlastP using both the NCBI  
473 (<https://blast.ncbi.nlm.nih.gov>) and JGI Mycosm  
474 (<https://mycosm.jgi.doe.gov/Podan3/Podan3.home.html>) databases.

475

## 476 **Acknowledgements**

477 This work was supported by a grant overseen by the French National Research Agency  
478 (ANR) as part of the "Investissements d'Avenir" program (ANR-11-LABX-0002-01, Lab of  
479 Excellence ARBRE) and the Region Lorraine Research Council. We thank Thomas Bacchetta  
480 for experimental help, Sylvie Cangemi for expert technical assistance, Christophe Rose (UMR  
481 SILVA-SILVATECH INRAE) for microscopy and Alexandre Kriznik for CD data  
482 (UMR7365 UL/CNRS IMoPA, Nancy, France). Proteomics analyses were performed on the  
483 PAPPSO platform (<http://pappso.inra.fr>) which is supported by INRA (<http://www.inra.fr>),  
484 the Ile-de-France regional council (<https://www.iledefrance.fr/education-recherche>), IBiSA (  
485 <https://www.ibisa.net>) and CNRS (<http://www.cnrs.fr>).

486

487 **The authors declare no competing interests.**

488

## 489 **References**

490 Aguilar-Zapata, D., Petraitiene, R., and Petraitis, V. (2015) Echinocandins: The Expanding  
491 Antifungal Armamentarium. Clin Infect Dis 61 Suppl 6:S604-11.

492

493 Alfaro, M., Oguiza, J.A., Ramírez, L., and Pisabarro, A.G. (2014) Comparative analysis of  
494 secretomes in basidiomycete fungi. *J Proteomics* 102: 28–43.  
495

496 Andersson, K.M., Meerupati, T., Levander, F., Friman, E., Ahrén, D., and Tunlid, A. (2013)  
497 Proteome of the nematode-trapping cells of the fungus *Monacrosporium haptotylum*. *Appl*  
498 *Environ Microbiol* 79: 4993-5004.  
499

500 Andersson, K.M., Kumar, D., Bentzer, J., Friman, E., Ahrén, D., and Tunlid, A. (2014)  
501 Interspecific and host-related gene expression patterns in nematode-trapping fungi. *BMC*  
502 *Genomics* 15: 968.  
503

504 Apetri, M.M., Maiti, N.C., Zagorski, M.G., Carey, P.R., and Anderson, V.E. (2006)  
505 Secondary Structure of  $\alpha$ -Synuclein Oligomers: Characterization by Raman and Atomic Force  
506 Microscopy. *J Mol Biol* 355 : 63–71.  
507

508 Baccelli, I., Luti, S., Bernardi, R., Scala, A., and Pazzagli, L. (2014) Cerato-platanin shows  
509 expansin-like activity on cellulosic materials. *Appl Microbiol Biotechnol* 98: 175–184.  
510

511 Ball, S.R., Kwan, A.H., and Sunde, M. (2020) Hydrophobin Rodlets on the Fungal Cell Wall  
512 *Curr Top Microbiol Immunol* 425: 29-51.  
513

514 Bang, K.H., Lee, D.W., Park, H.M., and Rhee, Y.H. (2000) Inhibition of fungal cell wall  
515 synthesizing enzymes by trans-cinnamaldehyde. *Biosci Biotechnol Biochem* 64: 1061-1063.  
516

517 Belkin, M., and Niyogi, P. (2003) Laplacian eigenmaps for dimensionality reduction and data  
518 representation. *Neural Comput* 15: 1373-1396.

519

520 Boucher, C., Nguyen, T.S., and Silar P. (2017) Species delimitation in the *Podospora*  
521 *anserina*/*P. pauciseta*/*P. comata* species complex (Sordariales). *Cryptogamie, Mycologie* 38:  
522 485-506.

523

524 Bouws, H., Wattenberg, A., and Zorn, H. (2008) Fungal secretomes—nature’s toolbox for  
525 white biotechnology. *Appl Microbiol Biotechnol* 80: 381-388.

526

527 Brun, S., Malagnac, F., Bidard, F., Lalucque, H., and Silar, P. (2009) Functions and regulation  
528 of the Nox family in the filamentous fungus *Podospora anserina*: a new role in cellulose  
529 degradation. *Mol Microbiol* 74: 480-96.

530

531 Bruneau, M., Mottet, T., Moulin, S., Kerbirou, M., Chouly, F., Chrétien, S., and Guyeux, C.  
532 (2018) A clustering package for nucleotide sequences using Laplacian Eigenmaps and  
533 Gaussian Mixture Model. *Computers in Biology and Medicine, Elsevier* 93: 66-74.

534

535 Cao, Y., Zhu, X., Jiao, R., and Xia, Y. (2012) The Magas1 gene is involved in pathogenesis  
536 by affecting penetration in *Metarhizium acridum*. *J Microbiol Biotechnol* 22 : 889–893.

537

538 Cock, P.A., Antao, T., Chang, J.T., Chapman, B.A., Cox, C.J., Dalke, A., *et al.* (2009)  
539 Biopython: freely available Python tools for computational molecular biology and  
540 bioinformatics. *Bioinformatics* 25: 1422-1423.

541

542 Dichtl, K., Helmschrott, C., Dirr, F., and Wagener, J. (2012) Deciphering cell wall integrity  
543 signalling in *Aspergillus fumigatus*: identification and functional characterization of cell wall  
544 stress sensors and relevant Rho GTPases. *Mol Microbiol* 83: 506-19.

545

546 Dynesen, J., and Nielsen, J. (2003) Surface hydrophobicity of *Aspergillus nidulans*  
547 conidiospores and its role in pellet formation. *Biotechnol Prog* 19: 1049-1052.

548

549 Feldman, D., Kowbel, D.J., Glass, N.L., Yarden, O., and Hadar, Y. (2017) A role for small  
550 secreted proteins (SSPs) in a saprophytic fungal lifestyle: Ligninolytic enzyme regulation in  
551 *Pleurotus ostreatus*. *Sci rep* 7: 14553.

552

553 Feldman, D., Amedi, N., Carmeli, S., Yarden, O., and Hadar, Y. (2019) Manipulating the  
554 expression of Small secreted protein 1 (Ssp1) alters patterns of development and metabolism  
555 in the white-rot fungus *Pleurotus ostreatus*. *Appl Environ Microbiol* 85: e00761-19.

556

557 Fernández-González, A.J., Valette, N., Kohler, A., Dumarçay, S., Sormani, R., Gelhaye, E.,  
558 and Morel-Rouhier, M. (2018) Oak extractive-induced stress reveals the involvement of new  
559 enzymes in the early detoxification response of *Phanerochaete chrysosporium*. *Environ*  
560 *Microbiol* 20: 3890-3901.

561

562 Frías, M., González, C., and Brito, N. (2011) BcSpl1, a cerato-platanin family protein,  
563 contributes to *Botrytis cinerea* virulence and elicits the hypersensitive response in the host.  
564 *New Phytol* 192: 483-495.

565

566 Futagami, T., Nakao, S., Kido, Y., Oka, T., Kajiwara, Y., Takashita, H., *et al.* (2011) Putative  
567 stress sensors WscA and WscB are involved in hypo-osmotic and acidic pH stress tolerance in  
568 *Aspergillus nidulans*. *Eukaryot Cell* 10: 1504-1515.

569

570 Gow, N.A.R., Latge, J.P., and Munro, C.A. (2017) The Fungal Cell Wall: Structure,  
571 Biosynthesis, and Function. *Microbiol Spectr* 5(3).

572

573 Grell, M.N., Mouritzen, P., and Giese, H. (2003) A *Blumeria graminis* gene family encoding  
574 proteins with a C-terminal variable region with homologues in pathogenic fungi. *Gene* 311:  
575 181–192.

576

577 Groenning, M. (2010) Binding mode of Thioflavin T and other molecular probes in the  
578 context of amyloid fibrils—current status. *J Chem Biol* 3: 1–18.

579

580 Huang, W., Hong, S., Tang, G., Lu, Y., and Wang, C. (2019) Unveiling the function and  
581 regulation control of the DUF3129 family proteins in fungal infection of hosts. *Philos Trans R*  
582 *Soc Lond B Biol Sci* 374: 20180321.

583

584 Justesen, A., Somerville, S., Christiansen, S., and Giese, H. (1996) Isolation and  
585 characterization of two novel genes expressed in germinating conidia of the obligate biotroph  
586 *Erysiphe graminis* f. sp. *hordei*. *Gene* 170: 131–135.

587

588 Kämper, J., Kahmann, R., Bölker, M., Ma, L.J., Brefort, T., Saville, B.J., *et al.* (2006) Insights  
589 from the genome of the biotrophic fungal plant pathogen *Ustilago maydis*. *Nature* 444: 97–  
590 101.

591

592 Kubicek, C.P., Baker, S.E., Gamauf, C., Kenerley, C.M., and Druzhinina, I.S. (2008)

593 Purifying selection and birth-and-death evolution in the class II hydrophobin gene families of

594 the ascomycete *Trichoderma/Hypocrea*. *BMC Evol Biol* 8: 4.

595

596 Kumar, S., Stecher, G., and Tamura, K. (2016) MEGA7: Molecular Evolutionary Genetics

597 Analysis version 7.0 for bigger datasets. *Mol Biol Evol* 33: 1870-1874.

598

599 Lashuel, H.A., Petre, B.M., Wall, J., Simon, M., Nowak, R.J., Walz, T., and Lansbury, P.T.

600 Jr. (2002) Alpha-synuclein, especially the Parkinson's disease-associated mutants, forms pore-

601 like annular and tubular protofibrils. *J Mol Biol* 322: 1089-1102.

602

603 Linder, M.B. (2009) Hydrophobins: Proteins that self assemble at interfaces. *Curr Opin*

604 *Colloid Interface Sci* 14: 356–363.

605

606 Luo, J., Wang, K., Li, G.S., Lei, D.Q., Huang, Y.J., Li, W.D., *et al.* (2018) 3,5-

607 Dicafeoylquinic Acid Disperses *Aspergillus Fumigatus* Biofilm and Enhances Fungicidal

608 Efficacy of Voriconazole and Amphotericin B. *Med Sci Monit* 24: 427-437.

609

610 Maddi, A., Dettman, A., Fu, C., Seiler, S., and Free, S.J. (2012) WSC-1 and HAM-7 are

611 MAPK-1 MAP kinase pathway sensors required for cell wall integrity and hyphal fusion in

612 *Neurospora crassa*. *PLoS ONE* 7: e42374.

613

614 Malavazi, I., Goldman, G.H., and Brown N.A. (2014) The importance of connections between  
615 the cell wall integrity pathway and the unfolded protein response in filamentous fungi. *Brief*  
616 *Funct Genomics* 13: 456-470.

617

618 Meerupati, T., Andersson, K.M., Friman, E., Kumar, D., Tunlid, A., and Ahrén, D. (2013)  
619 Genomic mechanisms accounting for the adaptation to parasitism in nematode-trapping fungi.  
620 *PLoS Genet.* 9: e1003909.

621

622 Mitchell, K.M., Zarnowski, R., and Andes, D.R. (2016) Fungal Super Glue: The Biofilm  
623 Matrix and Its Composition, Assembly, and Functions *PLoS Pathog* 12: e1005828.

624

625 Navarro, D., Couturier, M., Damasceno da Silva, G.G., Berrin, J-G., Rouau, X., Asther, M.,  
626 and Bignon, C. (2010) Automated assay for screening the enzymatic release of reducing  
627 sugars from micronized biomass. *Microbial Cell Fact* 9: 58.

628

629 Needleman, S., and Wunsch, C. (1970) A general method applicable to the search for  
630 similarities in the amino acid sequence of two proteins. *J Mol Biol* 48 : 443-53.

631

632 Nodet, P., Capellano, A., and Fèvre, M. (1990) Morphogenetic effects of Congo red on  
633 hyphal growth and cell wall development of the fungus *Saprolegnia monoka*. *J Gen Microbiol*  
634 136: 303-310.

635

636 Oliphant, T.E. (2006) A guide to NumPy, USA: Trelgol Publishing.

637

638 Pazzagli, L., Cappugi, G., Manao, G., Camici, G., Santini, A., and Scala, A. (1999)  
639 Purification, characterization, and amino acid sequence of cerato-platanin, a new phytotoxic  
640 protein from *Ceratocystis fimbriata* f sp platani. J Biol Chem 274: 24959–24964.  
641

642 Pellegrin, C., Morin, E., Martin, F.M., and Veneault-Fourrey, C. (2015) Comparative analysis  
643 of secretomes from ectomycorrhizal fungi with an emphasis on Small-Secreted Proteins.  
644 Front Microbiol 6: 1278.  
645

646 Piotrowski, J.S., Okada, H., Lu, F., Li, S.C., Hinchman, L., Ranjan, A., *et al.* (2015) Plant-  
647 derived antifungal agent poacic acid targets b-1,3-glucan. Proc Natl Acad Sci 112: E1490-7.  
648

649 Plett, J.M., Kemppainen, M., Kale, S.D., Kohler, A., Legué, V., Brun, A., *et al.* (2011) A  
650 secreted effector protein of *Laccaria bicolor* is required for symbiosis development. Curr Biol  
651 21: 1197–1203.  
652

653 Plett, J.M., Gibon, J., Kohler, A., Duffy, K., Hoegger, P.J., Velagapudi, R., *et al.* (2012)  
654 Phylogenetic, genomic organization and expression analysis of hydrophobin genes in the  
655 ectomycorrhizal basidiomycete *Laccaria bicolor*. Fungal Genet Biol 49 : 199–209.  
656

657 Ragni, E., Fontaine, T., Gissi, C., Latgè, J.P., and Popolo, L. (2007) The Gas family of  
658 proteins of *Saccharomyces cerevisiae*: characterization and evolutionary analysis. Yeast 24:  
659 297-308.  
660

661 Reynolds, D. (2015) Gaussian mixture models. Encyclopedia of biometrics 827-832.

662 Rizet, G. (1941) Sur l'analyse génétique des asques du *Podospora anserina*. C. R. Acad. Sci.  
663 Paris 212: 59-61.  
664

665 Rizet, G. (1952) Les phénomènes de barrage chez *Podospora anserina*. I. Analyse génétique  
666 des barrages entre souches S and s. Rev Cytol Biol Veg 13: 51-92.  
667

668 Ruocco, M., Lanzuise, S., Lombardi, N., Woo, S.L., Vinale, F., Marra, R., *et al.* (2015)  
669 Multiple roles and effects of a novel *Trichoderma* Hydrophobin. Mol Plant Microbe Interact  
670 28: 167–179.  
671

672 Schwarz, G.E. (1978) Estimating the dimension of a model. Annals of Statistics 6: 461–464.  
673

674 Semerdzhiev, S.A., Lindhoud, S., Stefanovic, A., Subramaniam, V., van der Schoot, P., and  
675 Claessens, M.M.A.E. (2018) Hydrophobic-Interaction-Induced Stiffening of Alpha-Synuclein  
676 Fibril Networks. Phys Rev Lett 120: 208102.  
677

678 Shang, Y., Xiao, G., Zheng, P., Cen, K., Zhan, S., and Wang, C. (2016) Divergent and  
679 convergent evolution of fungal pathogenicity. Genome Biol Evol 8: 1374–1387.  
680

681 Shanmugam, N., Baker, M.O.D.G., Ball, S.R., Steain, M., Pham, C.L.L., and Sunde, M.  
682 (2019) Microbial functional amyloids serve diverse purposes for structure, adhesion and  
683 defence. Biophys Rev 11: 287-302.  
684

685 Silar, P. (1995) Two new easy-to-use vectors for transformations. Fungal Genet News 1 42:  
686 73.

687  
688  
689  
690  
691  
692  
693  
694  
695  
696  
697  
698  
699  
700  
701  
702  
703  
704  
705  
706  
707  
708  
709  
710  
711

Silar, P. (2013) *Podospora anserina*: from laboratory to biotechnology. In: Genomics of Soil- and Plant-Associated Fungi. P. K. M. Benjamin A. Horwitz, Mala Mukherjee, Christian P. Kubicek (ed). Heidelberg New York Dordrecht London: Springer, pp. 283-309.

Thuillier, A., Chibani, K., Belli, G., Herrero, E., Dumarçay, S., Gérardin, P., *et al.* (2014) Transcriptomic responses of *Phanerochaete chrysosporium* to oak acetonic extracts: Focus on a new glutathione transferase. *Appl Environ Microbiol* 80: 6316–6327.

Tong, S.M., Chen, Y., Zhu, J., Ying, S.H., and Feng, M.G. (2016b) Subcellular localization of five singular WSC domain-containing proteins and their roles in *Beauveria bassiana* responses to stress cues and metal ions. *Environ Microbiol Rep* 8: 295-304.

Tong, S.M., Chen, Y., Ying, S.H., and Feng, M.G. (2016a) Three DUF1996 proteins localize in vacuoles and function in fungal responses to multiple stresses and metal ions. *Sci Rep* 6: 20566.

Tong, S.M., Wang, D.Y., Gao, B.J., Ying, S.H., Feng, M.G. (2019) The DUF1996 and WSC domain-containing protein Wsc1I acts as a novel sensor of multiple stress cues in *Beauveria bassiana*. *Cell Microbiol* 21: e13100.

Valette, N., Benoit-Gelber, I., Falco, M.D., Wiebenga, A., de Vries, R.P., Gelhaye, E., and Morel-Rouhier, M. (2017) Secretion of small proteins is species-specific within *Aspergillus* sp, *Microb Biotechnol* 10: 323–329.

712 Valette, N., Perrot, T., Sormani, R., Gelhaye, E., and Morel-Rouhier, M. (2017) Antifungal  
713 activities of wood extractives. *Fungal Biol Rev* 31: 113–123.  
714

715 Van Den Bossche, H. (2002) Echinocandins - an update. *Expert Opinion Ther Pat* 12: 151-  
716 167.  
717

718 Verna, J., Lodder, A., Lee, K., Vagts, A., and Ballester, R. (1997) A family of genes required  
719 for maintenance of cell wall integrity and for the stress response in *Saccharomyces cerevisiae*.  
720 *Proc Natl Acad Sci USA* 94: 13804-13809.  
721

722 Vincent, D., Kohler, A., Claverol, S., Solier, E., Joets, J., Gibon, J., *et al.* (2012) Secretome of  
723 the free-living mycelium from the ectomycorrhizal basidiomycete *Laccaria bicolor*. *J*  
724 *Proteome Res* 11: 157-171.  
725

726 Wessels, J.G., De Vries, O.M., Asgeirsdottir, S.A., and Schuren, F.H. (1991) Hydrophobin  
727 genes involved in formation of aerial hyphae and fruit bodies in *Schizophyllum*. *Plant Cell* 3:  
728 793-799.  
729

730 Wessels, J.G.H. (1996) Fungal hydrophobins: proteins that function at an interface. *Trends*  
731 *Plant Sci* 1: 9-15.  
732

733 Xue, C., Park, G., Choi, W., Zheng, L., Dean, R.A., and Xu, J.R. (2002) Two novel fungal  
734 virulence genes specifically expressed in appressoria of the rice blast fungus. *Plant Cell* 14:  
735 2107-2119.  
736

737 Zhang, B., Cai, J., Duan, C.Q., Reeves, M.J., and Fei He, F. (2015) A review of polyphenolics  
738 in oak woods. *Int J Mol Sci* 16: 6978-7014.

739

740 Zhu, N., Liu, J., Yang, J., Lin, Y., Yang, Y., Ji, L., *et al.* (2016) Comparative analysis of the  
741 secretomes of *Schizophyllum commune* and other wood-decay basidiomycetes during solid-  
742 state fermentation reveals its unique lignocellulose-degrading enzyme system. *Biotechnol*  
743 *Biofuels* 9: 42.

744

745 Zykwinska, A., Guillemette, T., Bouchara, J-P., and Cuenot, S. (2014) Spontaneous self-  
746 assembly of SC3 hydrophobins into nanorods in aqueous solution. *Biochimica et Biophysica*  
747 *Acta* 1844: 1231-1237.

748

#### 749 **Figure legends**

#### 750 **Fig. 1: Comparative genomics of fungal OSIP1**

751 Sequences were retrieved from the whole fungal JGI database (Mycocosm from Joint  
752 Genome Institute) using BlastP search tool with PcOSIP1, PaOSIP1 and P209725 as  
753 templates. (A) A total of 1057 sequences have been retrieved (cut off of  $E_{value}=10^{-5}$ ) and  
754 clustered as described in Experimental procedures part. The number of sequences found per  
755 trophic mode is indicated by various colors for each cluster. (B) Sequence alignment of  
756 ascomycete OSIP1 sequences from *P. anserina*, *Chaetomium thermophilum*, *Sordaria*  
757 *brevicollis* and *Fusarium solani*. The signal peptide of secretion is colored in yellow, the  
758 DUF3129 domain in blue gray. The eight conserved cysteinyl residues are highlighted (in red  
759 those that are both conserved in basidiomycete and ascomycete sequences and in orange those  
760 that are specifically conserved in ascomycetes sequences) (C) Evolutionary relationship of  
761 OSIP1 and DUF3129 containing proteins. The evolutionary history of OSIP1 cluster

762 sequences and DUF3129 containing sequences retrieved from the Pfam database, was inferred  
763 using the Neighbor-Joining method. Basidiomycete sequences are highlighted in gray. The  
764 functionally characterized proteins are reported. Sc: *Saccharomyces cerevisiae*, Mg:  
765 *Magnaporthe grisea*, Pc: *Phanerochate chrysosporium*, Pa: *Podospora anserina*, Bg:  
766 *Blumeria graminis*, Cg: *Colletotrichum gloeosporioides*. Because some of DUF3129-  
767 containing proteins are annotated as GAS-like proteins in the pfam database, GAS1  
768 (Glycolipid Anchored Surface) from *Saccharomyces cerevisiae* that has been well studied  
769 (Ragni *et al.*, 2007) and the GAS1 sequence of *P. chrysosporium*, were added to the analysis.

770

771 **Fig. 2: Growth phenotype of *PaOSIP1*<sup>Δ</sup> in presence of caspofungin.**

772 Wild type, *PaOSIP1*<sup>Δ</sup> mutant and a complemented strain (*PaOSIP1*<sup>Δ</sup>*\_PaOSIP1*) were grown  
773 in M2 medium as control (A) and M2 supplemented with caspofungin (500 ng/ml) (B) for 10  
774 days at 27°C (n=3). The pictures show fungal growth after 10 days.

775

776 **Fig. 3: SEM images of *PaOSIP1*<sup>Δ</sup> and WT hyphal network.**

777 Cryosections of mycelium were obtained as described in material and methods and visualized  
778 by scanning electron microscopy. Images shown in the figure correspond to the top left  
779 quarter of the whole images shown in supplemental data. The bar scale corresponds to 5 μm.  
780 The extracellular matrix has been manually colored in yellow, the merged images are shown  
781 in the middle panels. The single colored ECM is presented on the right panels.

782

783 **Fig. 4: Self-assembly of PcOSIP1.**

784 (A) Circular dichroism analysis of PcOSIP1 secondary structure. The spectrum was recorded  
785 in 50 mM phosphate buffer pH 8.0 with 66 μM of protein. PcOSIP1 spectrum shows signals  
786 at 190, 208 and 222 nm (B) Dynamic light scattering analysis of the oligomerization state of

787 PcOSIP1. The percentage of the various oligomers of PcOSIP1 in 30 mM Tris-HCl pH 8.0-  
788 200 mM NaCl buffer (Tris-NaCl buffer) and 50 mM phosphate buffer pH 8.0 (Phosphate  
789 buffer) is represented by black bars. Rh: hydrodynamic radii. (C) Atomic Force Microscopy  
790 height images of PcOSIP1 in Tris-NaCl buffer and Phosphate buffer. Size of AFM images: 3  
791  $\mu\text{m} \times 3 \mu\text{m}$ . (D) Macromolecular (1 and 2) and microscopic (3) views of the PcOSIP1 gel.

792

793 **Fig. 5: Growth phenotype of *PaOSIP1<sup>A</sup>* in presence of oak extractives.**

794 Growth kinetics of the wild type, *PaOSIP1<sup>A</sup>* mutant and a complemented strain  
795 (*PaOSIP1<sup>A</sup>\_PaOSIP1*) in M2 medium supplemented with oak extractives (2 mg/ml) (n=3). The  
796 pictures show fungal growth after 10 days.

797

798 **Fig. 6: Secretome analysis of *PaOSIP1<sup>A</sup>* in comparison to the wild type strain in presence**  
799 **of oak sawdust.**

800 (A) Global analysis of the amount of proteins specifically detected or more abundant ((PAI  
801 fold>2) in the secretome of each strain in presence of oak sawdust (the experimental set up is  
802 described in the experimental section). (B) Percentage of the proteins found specific or more  
803 abundant in *PaOSIP1<sup>A</sup>* within the total of the proteins identified for each functional class. (C)  
804 Number of glycoside hydrolases (GH) of each family detected in the secretomes of *PaOSIP1<sup>A</sup>*  
805 and wild type strains in presence of oak sawdust. The proportion of proteins detected as  
806 specific or more abundant (PAI fold>2) in the mutant strain is represented as red bars, the  
807 dark blue bars corresponding to the number of GH showing PAI fold<2 for the mutant  
808 compared to wild type. (D) Protein Abundance Index (PAI) for each strain. A focus has been  
809 made on cell wall-related proteins. ProtID are those from the JGI Mycomcom database. Full  
810 proteomic data are available in Table S2.

811

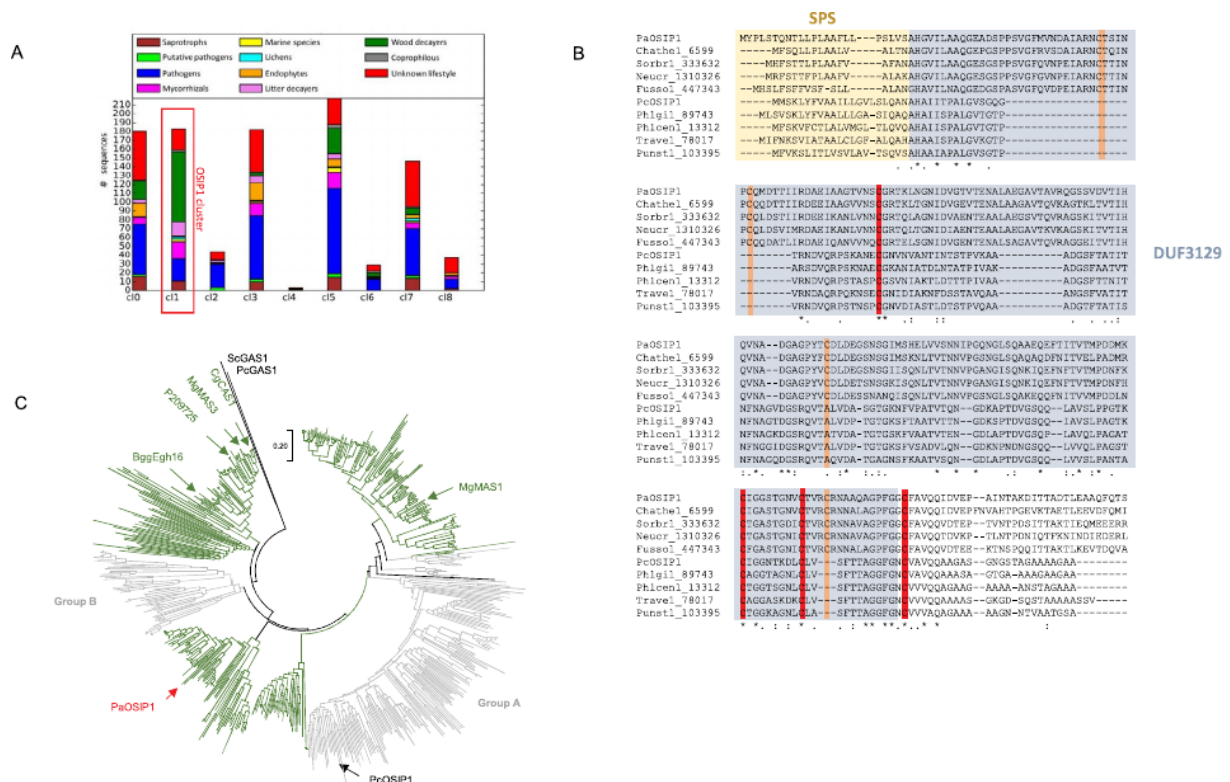
812 **Fig S1: Sequence alignment of basidiomycete OSIP1 sequences from *P. chrysosporium*,**  
 813 ***T. versicolor*, *Phlebiopsis gigantea*, *Punctularia strigosozonata* and *Phlebia centrifuga*.** The  
 814 signal peptide of secretion is colored in yellow, the DUF3129 domain in blue gray. The four  
 815 conserved cysteinyl residues are highlighted in red.

816

817 **Fig. S2: Strategy for PaOSIP1 deletion.** (A) Gene replacement strategy for deleting  
 818 *PaOSIP1* in *Podospora anserina*. (B) Primers used for gene replacement and probe synthesis  
 819 as described in the experimental procedures section. (C) Southern blot showing the efficiency  
 820 of the gene replacement and insertion of the resistance cassette in a single copy within the  
 821 genome. Genomic DNA was digested by Pst1 restriction enzyme and hybridized with both  
 822 AB and CD digoxigenin labeled probes.

823

824

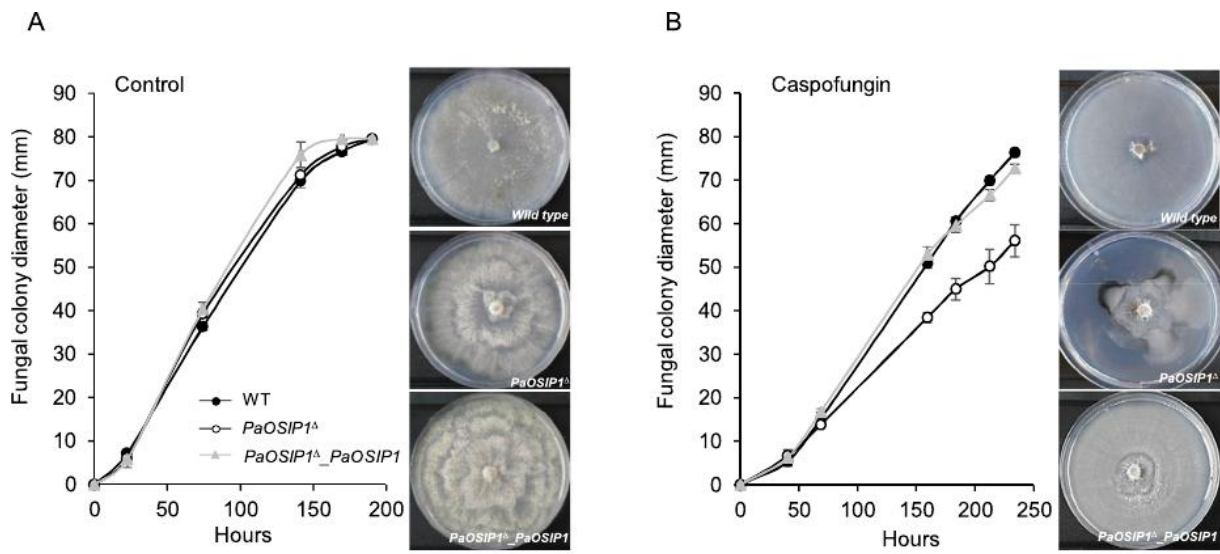


825

826

Figure 1

827



828

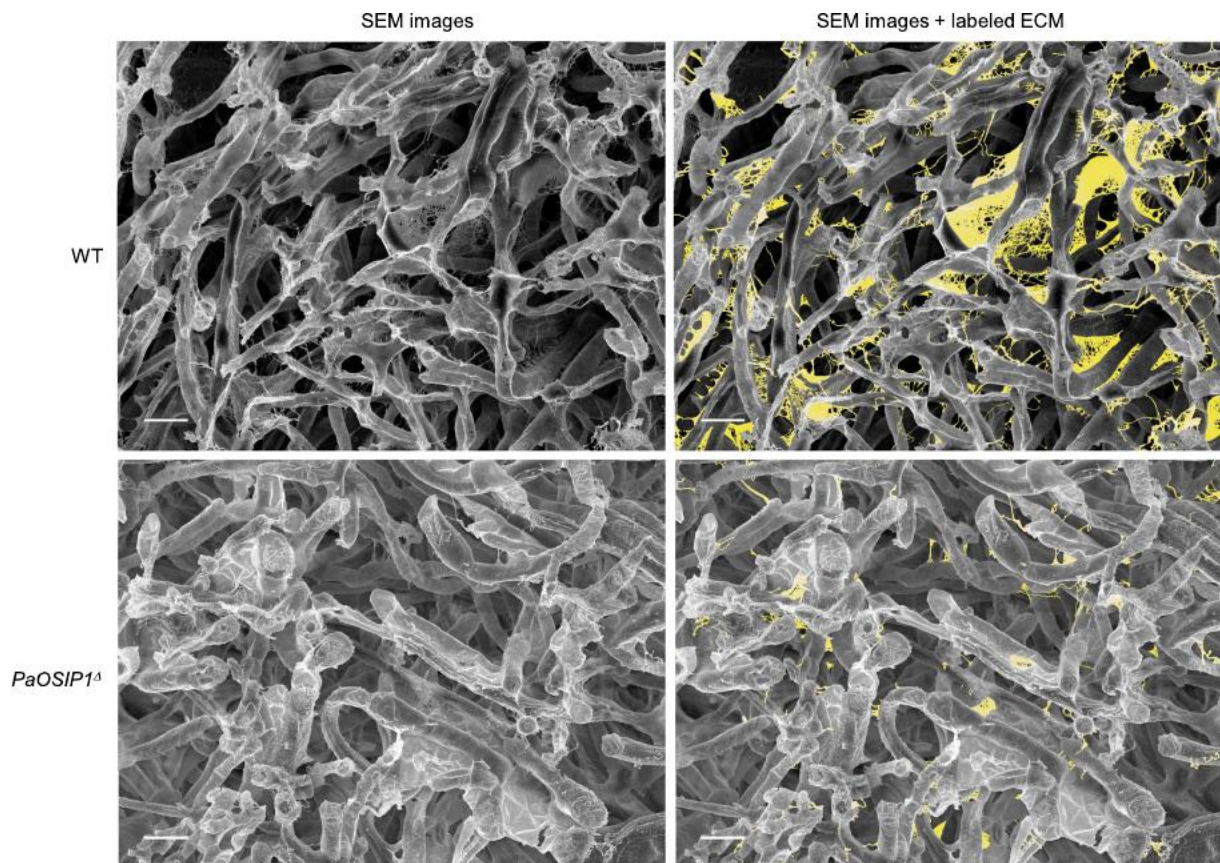
829

**Figure 2**

830

831

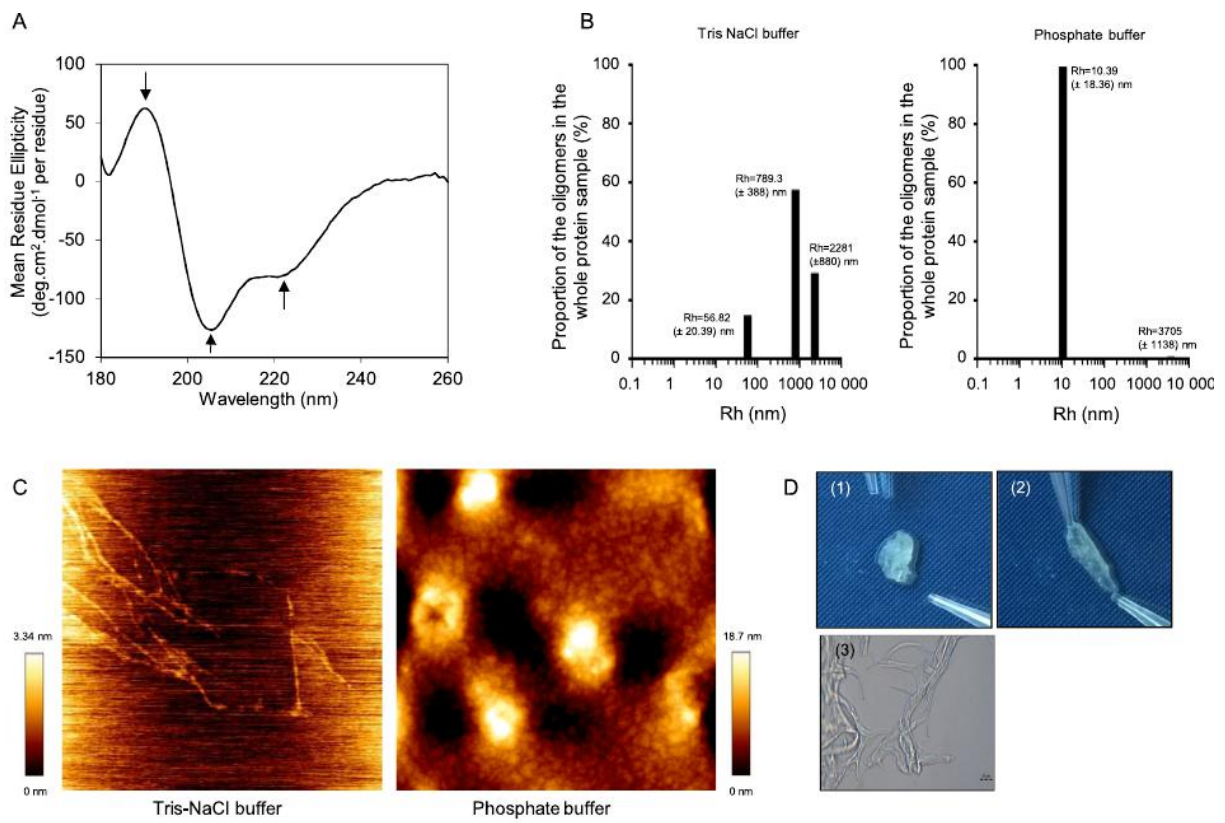
832



833

834

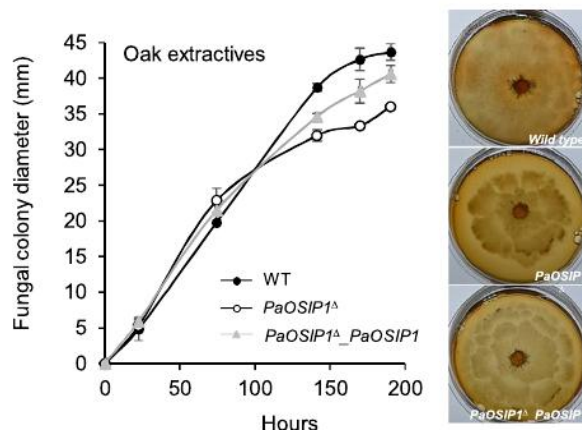
**Figure 3**



835

836

**Figure 4**

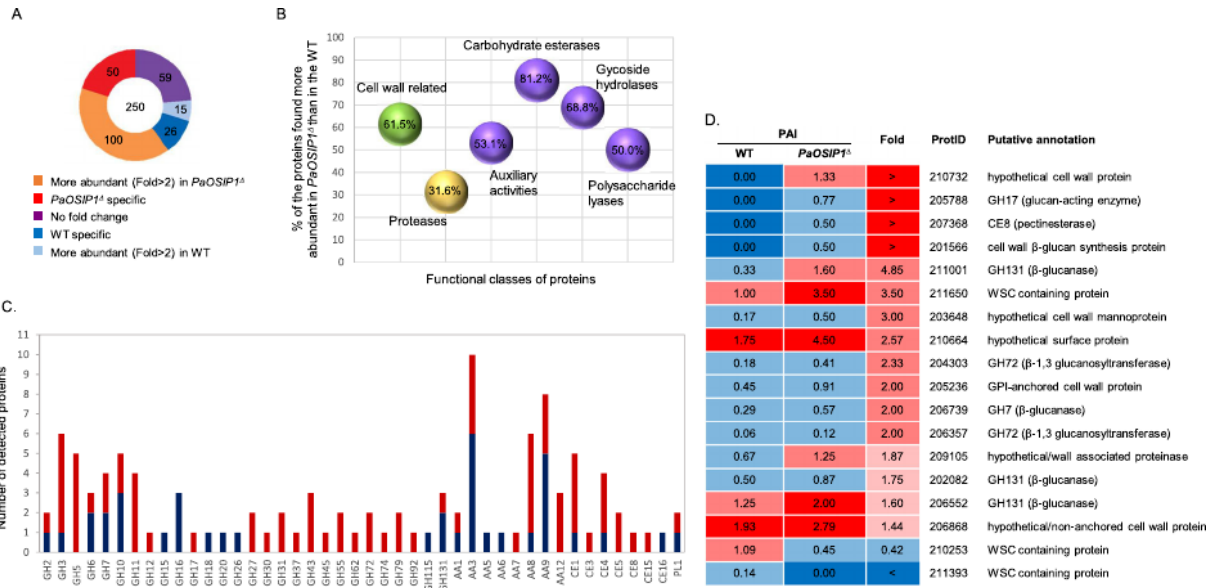


837

838

**Figure 5**

839



840

841

842

843

844

845

**Figure 6**